S & M 4210

Computational Fluid Dynamics Analysis of Electrode Material and Geometric Effects in Redox Flow Batteries

Cheng-Hsien Kuo,* Shang-Ching Chuang, and Hung-Yu Chen

Department of Mold and Die Engineering, National Kaohsiung University of Science and Technology, No. 415, Jiangong Rd., Sanmin Dist., Kaohsiung City 807618, Taiwan

(Received July 3, 2025; accepted October 17, 2025)

Keywords: redox flow battery, battery design, finite element analysis, computational fluid dynamics

The integration of renewable energy necessitates advanced storage solutions, with redox flow batteries (RFBs) exhibiting significant potential. However, conventional RFBs with enlarged electrode areas suffer from nonuniform electrolyte distribution, increasing internal resistance, and degrading performance. In this study, we address this limitation through a redesigned RFB structure incorporating graphite flow field plates and carbon felt electrodes. Finite element method simulations were performed to evaluate critical parameters: electrode area (10 cm²), polygonal geometry (hexagonal), and slope channel angle (7°). Results showed that this configuration—employing chemically resistant graphite for structural components and high-surface-area carbon felt for electrodes—optimizes the flow field distribution uniformity. The 7°-sloped hexagonal channels significantly reduce flow maldistribution compared with traditional designs. This geometric and material optimization directly enhances electrochemical performance by mitigating resistance issues, providing a viable approach for scaling RFB systems.

1. Introduction

Although the discovery of energy resources has catalyzed the Industrial Revolution and spurred advancements in science and technology, global energy demand has continued to rise in tandem with increasing energy consumption. This growing demand has resulted in elevated carbon emissions, primarily owing to the extensive use of finite fossil fuels such as coal, oil, and natural gas. On the other hand, renewable energy exhibits unstable power generation dependent on the natural environment and geographical conditions. Therefore, to solve this problem, energy storage system (ESS) devices must be used to allocate and dispatch power effectively to maintain grid stability and energy allocation requirements. ESS devices can be classified into mechanical, chemical, electrochemical, electrical, and thermal categories on the basis of the form of energy stored in them. Electrochemical energy storage devices include lithium batteries, lead-acid batteries, sodium-sulfur batteries, and redox flow batteries (RFBs). RFBs are easier to recycle than lead-acid batteries; additionally, RFBs have the advantages of high safety, long cycle life, and good stability compared with lithium batteries.

*Corresponding author: e-mail: chuckkuo@nkust.edu.tw https://doi.org/10.18494/SAM5838

RFBs store electricity through redox reactions among active materials constituting electrolytes. They are classified into various types according to the different electrolytes, such as vanadium, iron/chromium, vanadium/bromine, zinc/bromine, and zinc/nickel, and their output characteristics depend on the redox reaction of each electrolyte. Furthermore, RFBs can be customized for specific applications, demonstrating good flexibility in system design. Because the size of the stack that determines its output power and the size of the electrolyte storage tank that determines its energy storage capacity are separated and independent of each other, RFBs are suitable for large-scale ESS devices. (6–9) The operating current and voltage determine the output power of the batteries. To increase the output power of the batteries, enlarging the electrode area and increasing the number of batteries in series are the traditional design methods of the battery stack. When the electrode area is enlarged owing to the increase in the required operating current, the electrolyte is often unevenly distributed in the electrode area, resulting in improper electrolyte circulation. (10,11)

The performance of an RFB depends on several factors, including the battery geometry, flow field channel size, flow velocity, and charge/discharge rate. Traditionally, the flow field design and inlet/outlet position were changed, while the typical square battery geometry was maintained. Therefore, the battery geometry has yet to be thoroughly studied. In recent years, advancements in the output power and efficiency of RFBs have been achieved primarily through structural optimization and the refinement of flow channel designs in the channel frame plate. For example, the structural optimization achieved through geometric design, along with the incorporation of sloped flow channels, can enhance the uniform distribution of electrolytes within the electrode reaction region and expand the effective active surface area, thereby maximizing the actual reaction output of RFBs. In this study, to consider factors such as electrode area, geometric structure, and slope channel angle, COMSOL Multiphysics 5.6 was used to calculate and compare the velocity field of the RFB model. Moreover, the uniformity of the internal flows of the electrode geometric model was discussed to select the best design.

2. Experimental Procedure

2.1 Governing equations

The set physical quantity was considered to be the porous media in the reaction area of the central electrode. It is described on the basis of Darcy's law, as shown in Eq. (1). The remaining inlet and outlet channels were free-flow areas regarded as comprising a single-phase fluid in the laminar flow. This is described by the Navier–Stokes equation, as shown in Eq. (2). The basic equation of fluid mechanics can be used to describe the flow of fluid in this area.⁽¹⁷⁾

$$v = (k / \mu \varepsilon) \nabla p \tag{1}$$

$$\rho(v \cdot \nabla)v = -p + \mu \left[\nabla v + (\nabla v)^{\mathrm{T}} \right]$$
 (2)

Here, v is the fluid velocity (m/s), k is the permeability (m²) of porous media, μ is the dynamic viscosity coefficient (Pa-s), ε is the porosity, p is the pressure (Pa), and ρ is the fluid density (kg/m³).

2.2 RFB geometries

The battery model structure used in this study was based on the battery's traditional flow channel frame plate. The traditional battery comprises vertically symmetrical flow channels and electrodes, and carbon felt with a reaction area of 100 cm^2 ($10 \times 10 \text{ cm}^2$) was used as the electrode material. The electrolyte in the flow field model structure has a Z-type flow, which enters from the lower left inlet, flows through the main channel, enters the electrode reaction area through the subchannel, and finally flows out from the upper right outlet. The thickness (4.50 mm) of the electrode, the depth (1.00 mm) and width (2.00 mm) of the main channel, and the length (3.00 mm) and width (1.50 mm) of the subchannel remained unchanged (Fig. 1).

First, eight design models with different electrode reaction areas of 1, 5, 10, 25, 50, 100, 200, and 600 cm² were designed [Figs. 2(a)–2(h)]. Square electrodes are widely used in experiments and simulations as a standardized geometric reference. Their design ensures the generalizability and comparability of results, enabling direct comparison between studies. The mean flow velocities at 25 discrete points within each region were calculated to evaluate the effect of electrode area on flow field uniformity [Fig. 3(a)]. From the simulation results of different electrode areas of 1, 5, 10, 25, 50, 100, 200, and 600 cm², the polygonal structural design was determined using the optimal flow velocity corresponding to each electrode area. Then, three design models with square, diamond, and hexagonal structures were compared on the basis of different polygon geometries. The mean flow velocities at equally divided points in each area were calculated to compare the effects of different polygon geometries on the flow field uniformity, as shown in Figs. 3(a)–3(c).

Finally, from the simulation results of square, diamond, and hexagonal structure design models with different polygon geometry structures, we determined the flow channel angles with

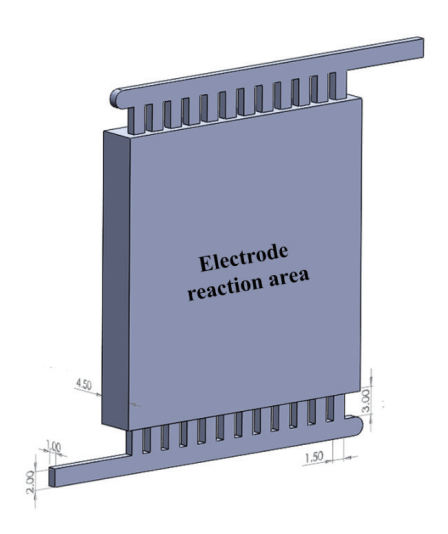


Fig. 1. (Color online) Flow field model size.

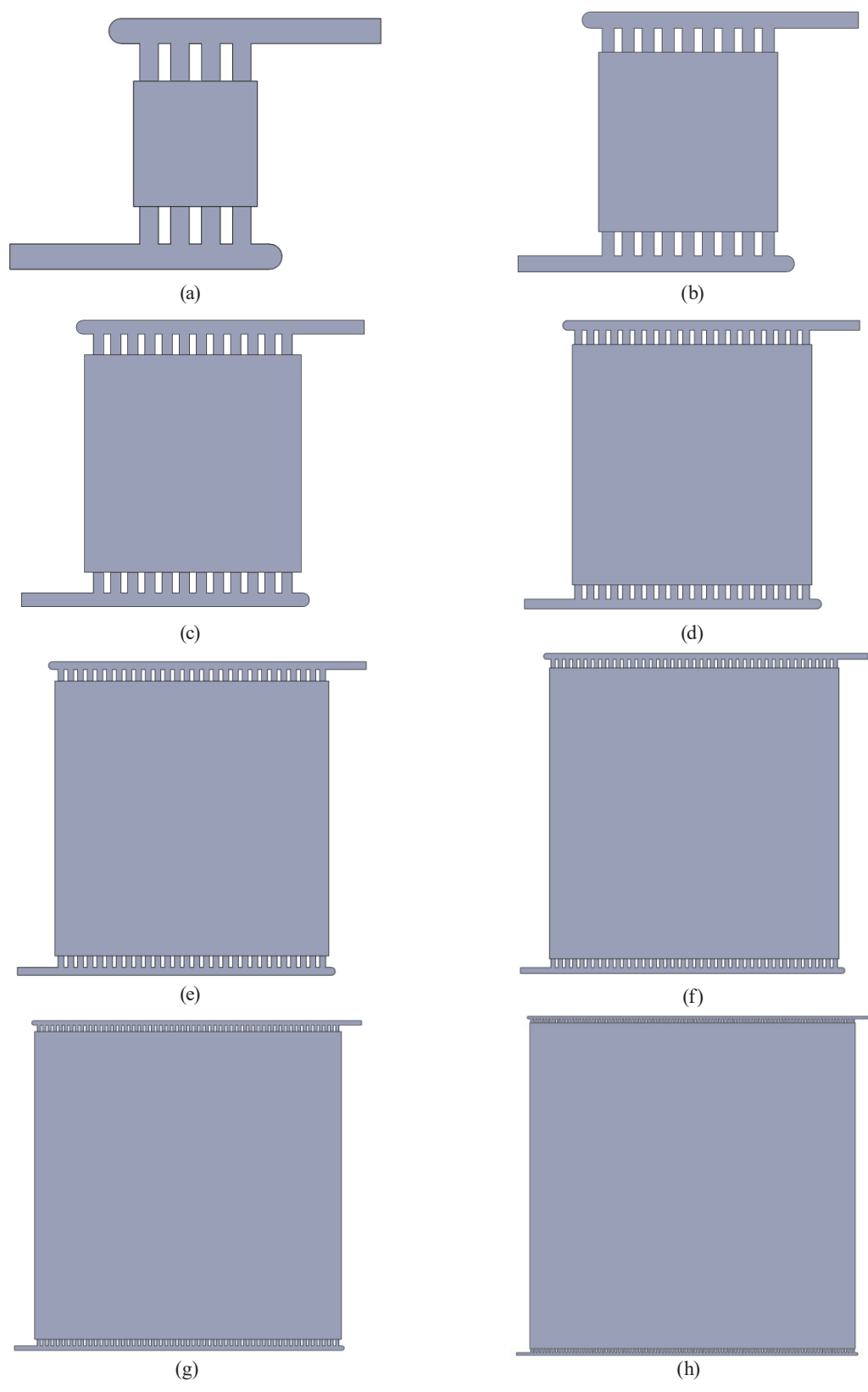


Fig. 2. (Color online) Design models with electrode reaction areas of 1, 5, 10, 25, 50, 100, 200, and 600 cm².

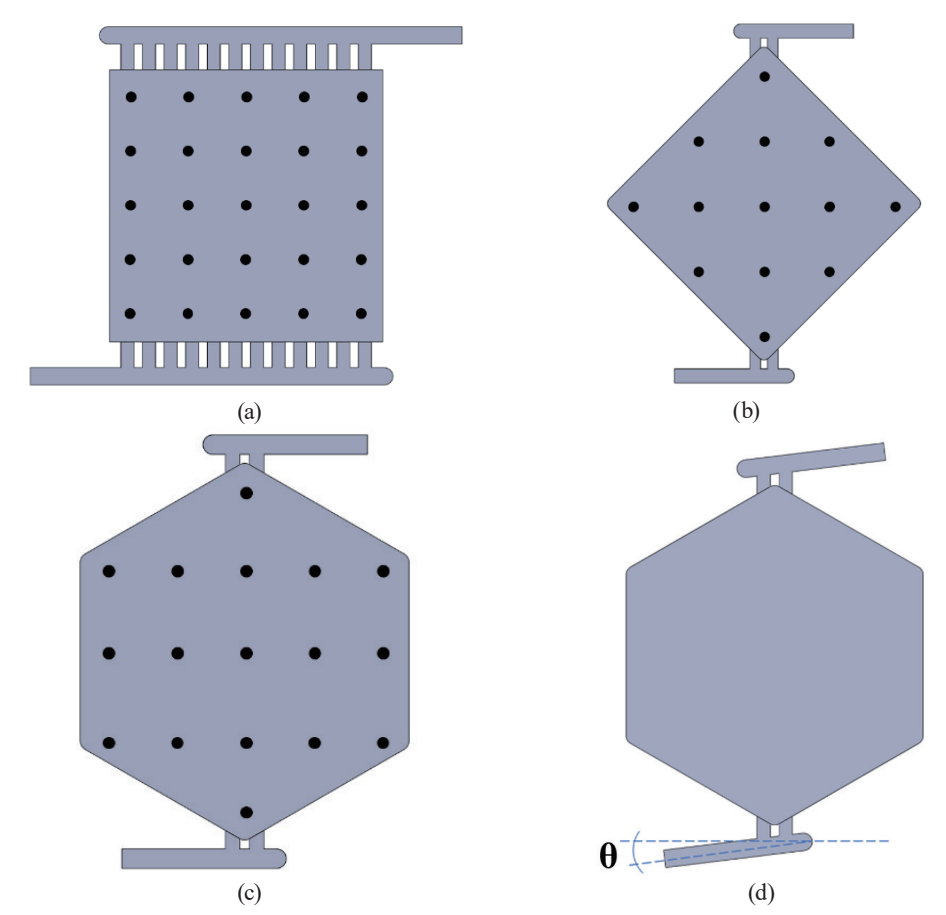


Fig. 3. (Color online) Schematic diagram of models with different polygon geometries and slope angles.

different slopes using the optimal values of the different polygon geometry structures. Then, a total of 21 sets of design models were designed with angles ranging from 0 to 10° increasing in steps of 0.5° in accordance with the different slope channel angle designs. As shown in Fig. 3(d), the mean flow velocity, the standard deviation of mean flow velocity, and the flow resistance in the electrode area were calculated on the basis of the simulation numerical results to compare the effects of different slope channel angle design values on flow field uniformity.

2.3 Numerical details

To reduce computational requirements, simplified boundary conditions were applied in the three-dimensional simulation model for half-cell fluid dynamics and flow field analysis (Fig. 4). For the different electrode areas, the velocity at the electrolyte inlet was customized on the basis of the 2 ml/min flow rate per square area (Table 1). The electrolyte outlet was set as the atmospheric pressure outlet boundary, while all remaining wall boundaries were specified to be under no-slip conditions. The flow field simulation parameters are shown in Table 2.⁽¹⁸⁾ Regarding model assumption, the basic equations of fluid mechanics can be used to describe the fluid flow in this area. Moreover, the simulation analysis is predicated on the assumption that the electrolyte flow rate in the vanadium RFB has saturated under prolonged, stable operating conditions. The basic assumptions of this model are as follows.⁽¹⁹⁾

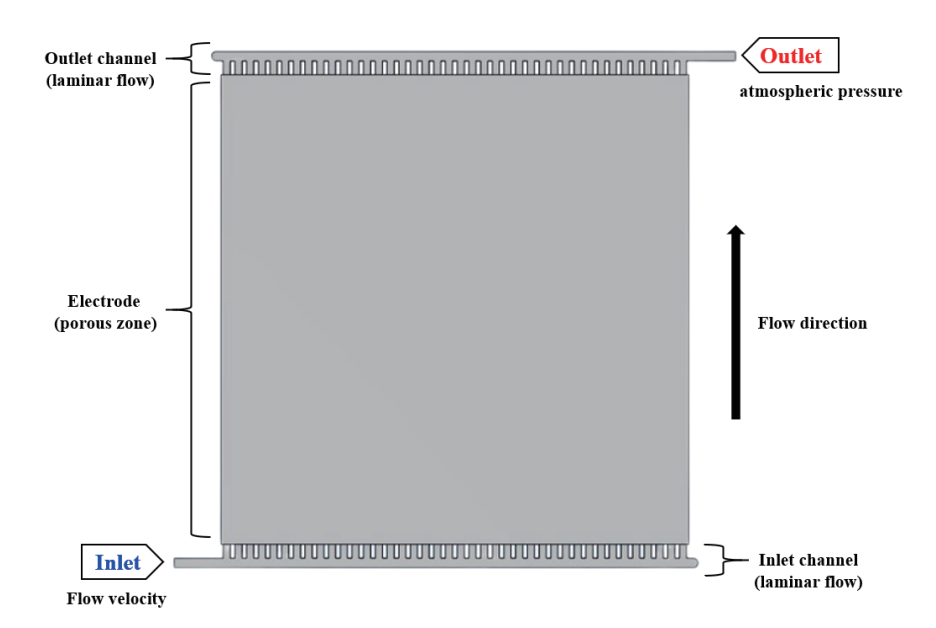


Fig. 4. (Color online) Boundary condition settings for flow field analysis.

Table 1 User-defined inlet flow velocities for different electrode areas.

Electrode area	Flow per square area	Total flow	Inlet flow velocity
(cm^2)	(ml/min)	(m ³ /min)	(m/s)
1	2	3.33×10^{-8}	0.017
5	10	1.67×10^{-7}	0.083
10	20	3.33×10^{-7}	0.167
25	50	8.33×10^{-7}	0.417
50	100	1.67×10^{-6}	0.833
100	200	3.33×10^{-6}	1.667
200	400	6.67×10^{-6}	3.333
600	1200	2.00×10^{-5}	10.000

Table 2 Flow field simulation parameters. (18)

Symbol	Material property	Value	Unit
ρ	Fluid density	1300	kg/m ³
μ	Dynamic viscosity coefficient	4.93E-3	Pa-s
3	Porosity of carbon felt	0.93	_
κ	Permeability of carbon felt	8.625E-9	m^2
T	Temperature	298	K
p	Out pressure	0	Pa

- (1) The electrolyte is an incompressible flow.
- (2) The viscosity coefficient and fluid density are constant.
- (3) The porosity of porous carbon felt is uniformly distributed.
- (4) The effects of the gravity and temperature fields can be ignored.

3. Results and Discussion

Because the electrolyte distribution considerably affects the uniformity of the internal flow field and the electrode reaction area is the main place for the electrochemical reaction, the electrolyte distribution is a key factor affecting the battery performance. In this study, the geometric model design of the electrode was mainly modified, and the effects of electrode area, polygon geometry, and slope channel angle as well as the simulation results obtained on the basis of the different influential factors mentioned above were analyzed and are discussed below.

3.1 Effects of electrode area on electrolyte distribution

The flow velocity distributions within the electrode reaction regions were analyzed and compared across design models with electrode areas of 1, 5, 10, 25, 50, 100, 200, and 600 cm². The streamline direction in the electrode area showed a diagonal flow trend from the bottom left to the top right, and the flow velocity also decreased with the change in flow trend direction; the main reason was that there is flow inertia when the electrolyte flows from the inlet to the outlet. As a result, the flow velocity of the electrolyte is higher in the left half than in the right half of the electrode area. The flow velocity distributions for different areas, as shown in Fig. 5, reveal that the velocity at the electrolyte inlet in the lower left corner of the electrode area is maximum. The velocity at the opposite corner of the electrolyte inlet in the lower right corner is minimum, indicating that it is perpendicular to the direction of the electrolyte flow. The length of the main channel and the number of subchannels made it impossible for the electrolyte to enter the electrode area from left to right at the same time, so the electrolyte could only flow through a specific area, resulting in the uneven distribution of the flow field; therefore, a dead zone is easily formed. Consequently, the velocity of the electrolyte cannot be updated in a timely manner and the supply of active substances is incomplete in the low-velocity area.

Table 3 presents the flow velocity distribution data for different electrode areas, with mean velocities calculated from 25 equally divided sampling points within each area. The results indicate that the mean flow velocities corresponding to electrode areas of 1, 5, 10, 25, 50, 100, 200, and 600 cm² are 0.18, 0.42, 0.82, 1.21, 2.58, 3.61, 7.8, and 14.9 mm/s, respectively. Similarly, the flow velocity differences for these areas are 0.2, 1.16, 2.29, 4.79, 11.1, 20.8, 55.3, and 88.6 mm/s, respectively. The trend diagram of the mean flow velocity and the upper and lower limits of the flow velocity in different areas, as shown in Fig. 6, reveals that the mean flow velocity is linear for areas smaller than 10 cm², and the mean flow velocity continues to decrease with an increase in electrode area. The trend diagram of the flow velocity difference in different areas, as shown in Fig. 7, reveals that the flow velocity difference tends to be linear for electrode areas smaller than 25 cm²; the larger the electrode area, the greater the flow velocity difference. The comparative analysis indicated that the optimal electrode area was 10 cm²; therefore, the electrode area of 10 cm² was selected as the representative reaction area for subsequent investigations.

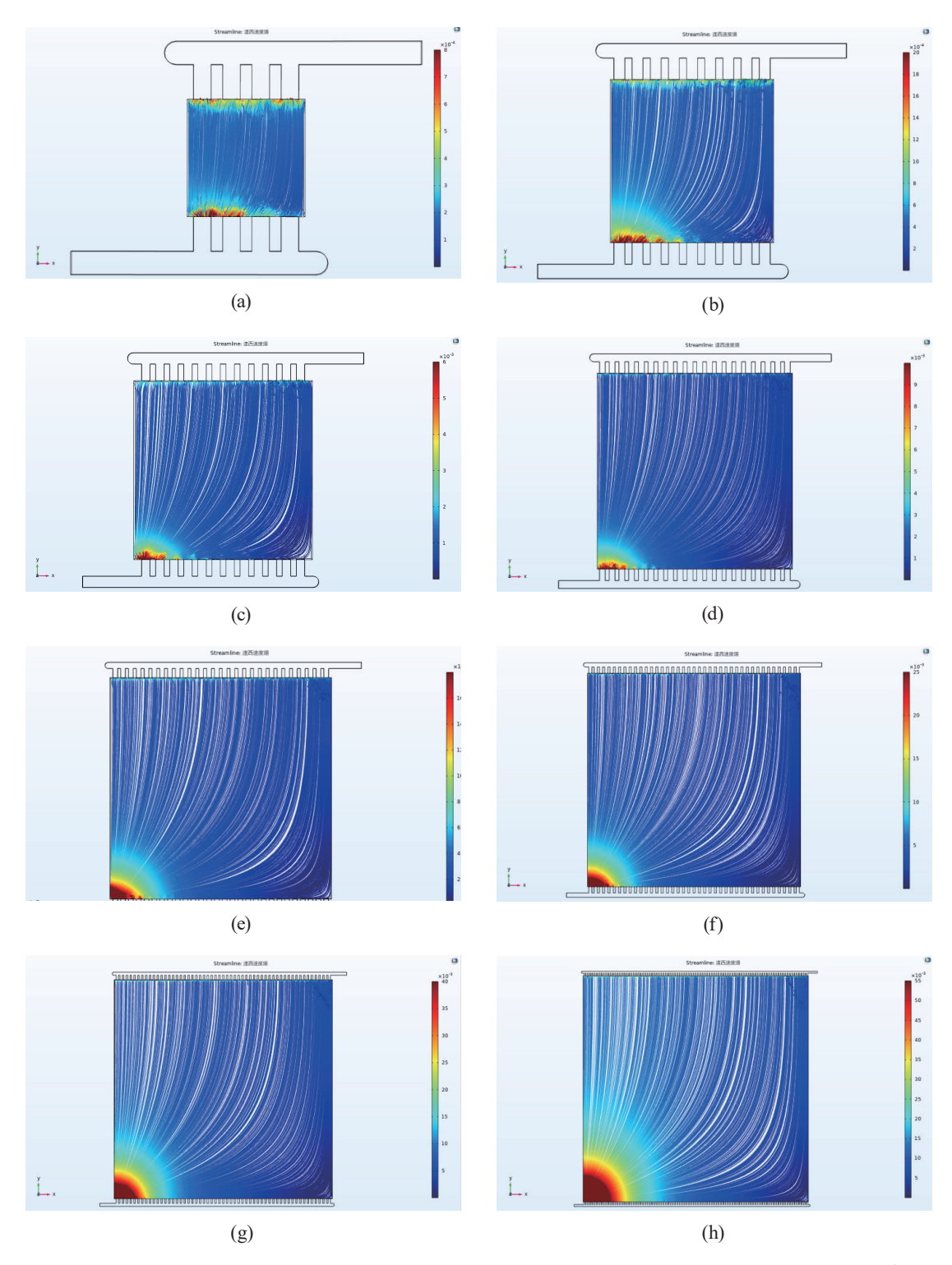


Fig. 5. (Color online) Velocity distributions for electrode areas of 1, 5, 10, 25, 50, 100, 200, and 600 cm².

Table 3
Data for different electrode areas.

Electrode area	Mean flow velocity	Max. flow velocity	Min. flow velocity	Flow velocity
(cm^2)	(mm/s)	(mm/s)	(mm/s)	difference (mm/s)
1	0.18	0.31	0.11	0.20
5	0.42	1.27	0.11	1.16
10	0.82	2.51	0.22	2.29
25	1.21	5.01	0.22	4.79
50	2.58	11.6	0.5	11.1
100	3.61	21.3	0.5	20.8
200	7.80	56.3	1.0	55.3
600	14.29	90.6	2.0	88.6

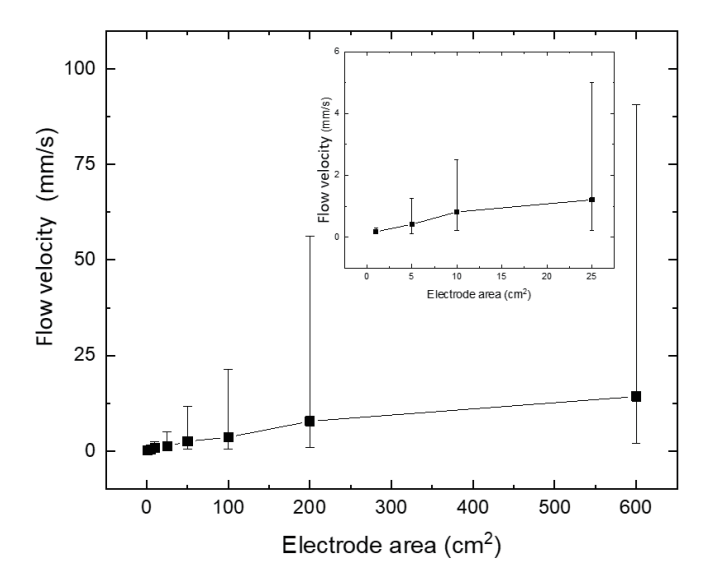


Fig. 6. Trends of mean flow velocity and upper and lower limits of flow velocity for different electrode areas.

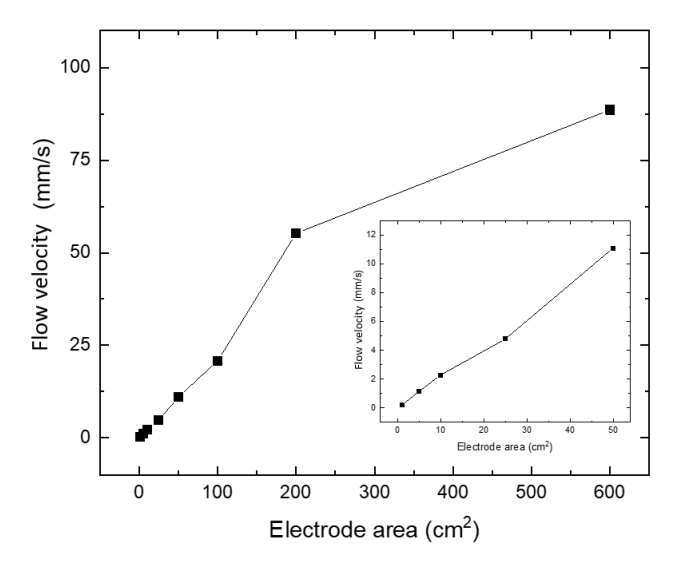


Fig. 7. Trend of flow velocity difference for different electrode areas.

3.2 Effects of different polygon geometries on electrolyte distribution

The electrode reaction area of 10 cm² determined the polygonal structure design. Different geometries of the polygonal design models, including square, diamond, and hexagonal structures, were used for data comparison. Figures 5 and 8 show the flow velocity distributions of various model designs in the electrode reaction region. The typical square structure of a flow battery presents a diagonal flow trend in the electrode area from the bottom left to the top right. The flow velocity decreases in accordance with the direction of the flow trend. The simulation results showed that there is significant pressure at the electrolyte inlet in the high-flow-velocity area of the model, which leads to a significant flow velocity difference compared with the lowflow-velocity area, resulting in an uneven distribution of the flow field, which is improved through the modification of structural geometry, that is, the modification of the streamline direction from the bottom left to the top right to a bottom-up flow trend direction, forming a diamond structure. The flow velocity distribution exhibited a relatively uniform pattern, symmetric about the central axis. Because the simulation results showed the minimum flow velocity on both sides of the center of the model, the places with the minimum flow velocity, such as the corners on both sides of the center, were removed so that the polygonal geometry forms a hexagonal structure, which is helpful in improving the overall mean flow velocity in the electrode area and in further improving the uniformity of the flow field distribution.

Combined with the data comparison of different polygon geometries, the mean flow velocity of different polygon geometries was improved from 0.82 to 1.21 mm/s through the modification of the geometries. The flow velocity difference of different polygon geometries was reduced from 2.29 to 1.47 mm/s. From the comparison of the velocity distributions in different polygon geometries (Fig. 9), the hexagonal structure was selected as the electrode geometry after model modification. The results showed that the overall mean velocity is improved and the maximum and minimum velocities are closer to the median, which indicates that the uniformity of the flow field distribution can be improved.

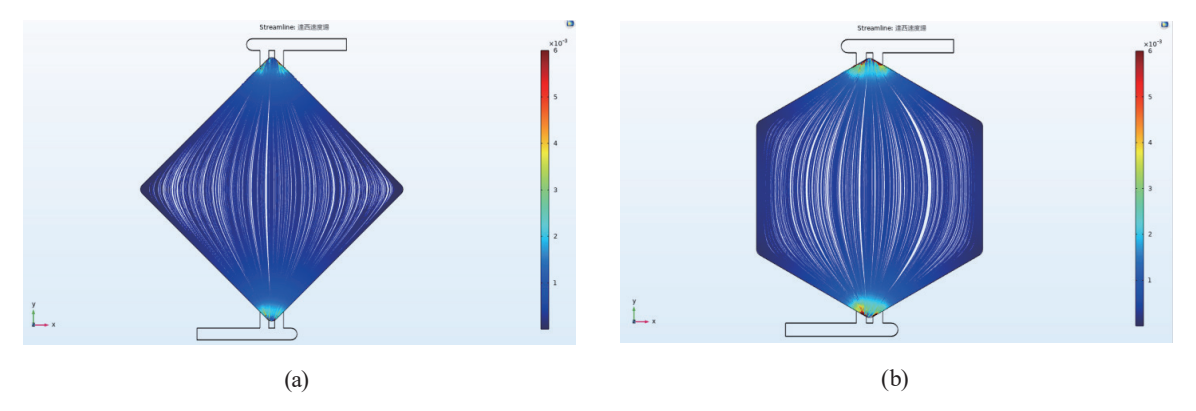


Fig. 8. (Color online) Flow velocity distributions of diamond and hexagonal structures.

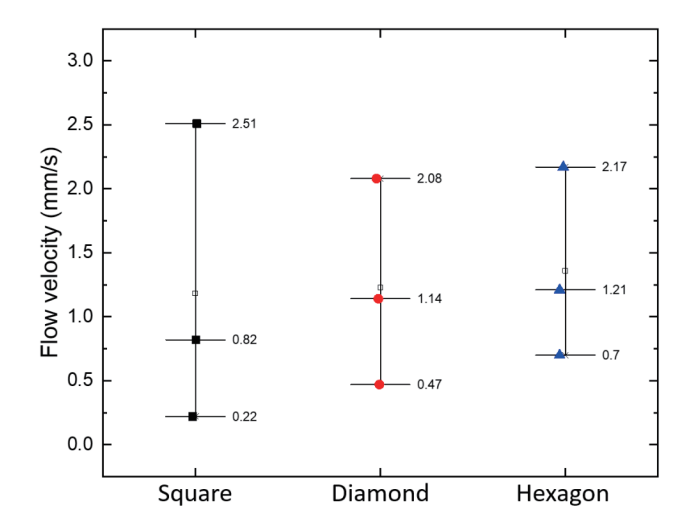


Fig. 9. (Color online) Velocity distributions of different polygon geometries (10 cm²).

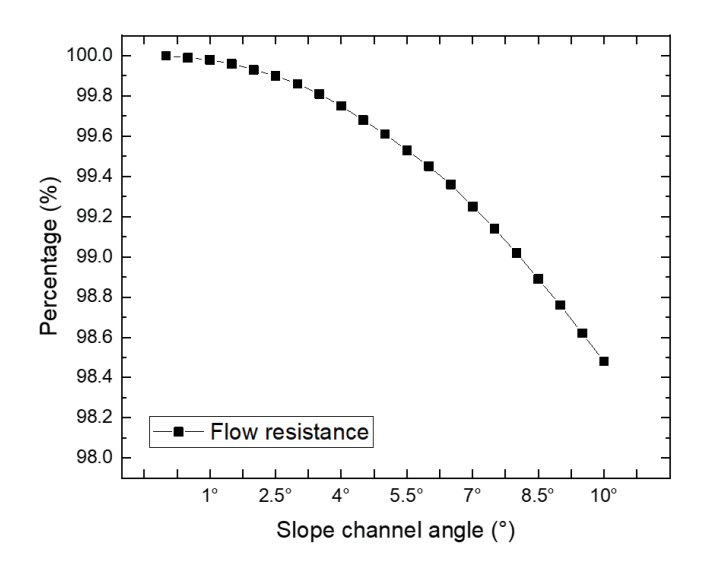


Fig. 10. Trend chart of flow resistance with different slopes.

3.3 Effects of different slope channel angles on electrolyte distribution

A total of 21 sets of design models were designed with angles ranging from 0 to 10° increasing in steps of 0.5° in accordance with different slope channel angle designs. The simulation results demonstrated that the various channel slope angles yielded relatively uniform flow velocity distributions across the entire flow field model as well as within the electrode region. When the slope flow angle was changed, the mean flow velocity in the electrode area changed minimally, approximately 1.21 mm/s; the sharp velocity gradient mainly occurs in the flow channel. The larger the channel angle, the lower the flow resistance (Fig. 10). The results showed that the slope channel angle of 7° is the optimal design value, and the minimum standard deviation of the mean flow velocity is 0.389, indicating that the flow velocity difference is relatively small (Fig. 11).

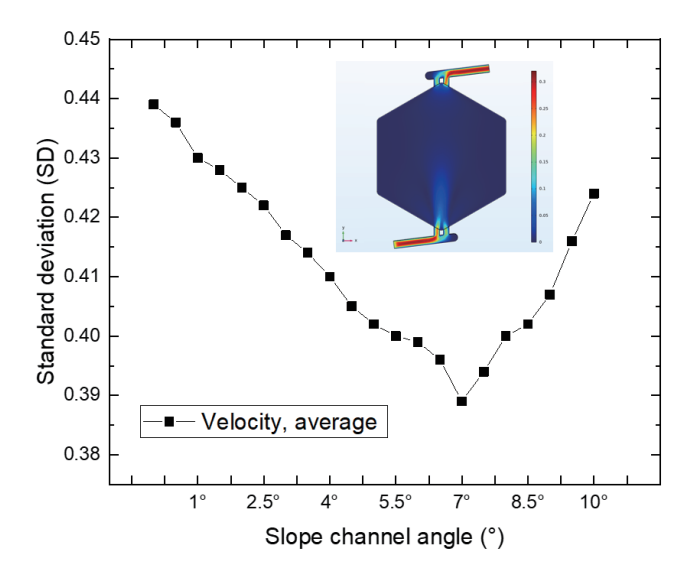


Fig. 11. (Color online) Trend chart of standard deviation of mean flow velocity with different slopes.

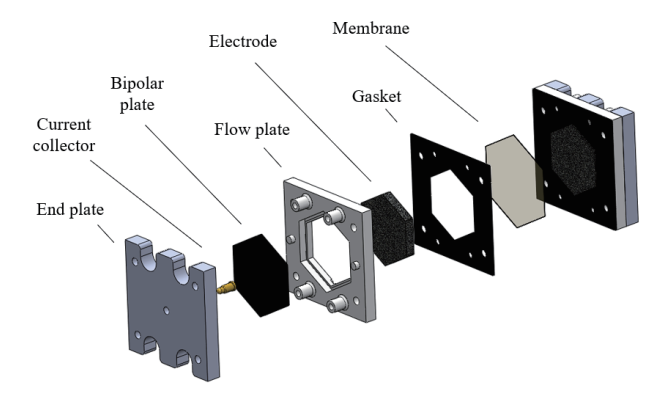


Fig. 12. (Color online) Design combination of new battery modules.

In summary, the new battery design has a hexagonal electrode area of 10 cm² and a slope channel angle of 7°, as shown in Fig. 12. The stack is assembled by arranging and combining independent single cells. The operating voltage can be achieved by connecting the single cells in series to achieve the required target or by connecting the single cells in parallel to achieve the necessary operating current.

4. Conclusions

The flow characteristics of RFBs were simulated and analyzed, and the effect of electrode model geometry on electrolyte distribution was described. The design of the batteries can considerably improve the uniformity of the flow field distribution and address the uneven distribution of electrolytes in the electrode reaction area that occurs with the traditional square geometry. The optimal design values of the new batteries in this study were as follows: an electrode area of 10 cm², a hexagonal structure as the polygon geometry, and a slope channel angle of 7°.

Through the design of the battery flow channel frame plate and fluid simulation analysis technology, the improper circulation of electrolytes caused by the uneven distribution of electrolytes in the electrode area of a traditional large-area flow battery is prevented, reducing the mean velocity error and flow resistance in the electrode area and improving the uniformity of the flow field distribution. The finite element method was used for numerical computation, and the geometry of the proposed optimized structure was found to be a promising alternative to the traditional RFB design. Experimental verification can be conducted in the future to assess the predicted flow distribution and its impact on RFB performance. The novel battery module, which allows the flexible stacking of individual cells in series for higher voltage or in parallel for increased current, enables adaptable system configurations to meet diverse application requirements. This flexibility will facilitate the comprehensive evaluation of the module's performance under various operating conditions and system designs.

Acknowledgments

This study was conducted under the industry-academia collaboration project 113A00182, which was supported by ShenEnergy Tech Ltd.

References

- 1 J. E. T. Bistline: Joule 5 (2021) 2551. https://doi.org/10.1016/j.joule.2021.09.012
- A. Ahmed, T. Ge, J. Peng, W.-C. Yan, B. T. Tee, and S. You: Energy Build. 256 (2022) 111755. https://doi.org/10.1016/j.enbuild.2021.111755
- 3 M. Stecca, L. R. Elizondo, T. B. Soeiro, P. Bauer, and P. Palensky: IEEE Open J. Ind. Electron. 1 (2020) 46. https://doi.org/10.1109/OJIES.2020.2981832
- 4 A. Parasuraman, T. M. Lim, C. Menictas, and M. Skyllas-Kazacos: Electrochim. Acta. 101 (2013) 27. https://doi.org/10.1016/j.electacta.2012.09.067
- 5 M. Gencten and Y. Sahin: Int. J. Energy Res. 44 (2020) 7903. https://doi.org/10.1002/er.5487
- 6 B. R. Chalamala, T. Soundappan, G. R. Fisher, M. R. Anstey, V. V. Viswanathan, and M. L. Perry: Proc. IEEE 102 (2014) 976. https://doi.org/10.1109/JPROC.2014.2320317
- 7 C. Ponce de León, A. Frías-Ferrer, J. González-García, D. A. Szánto, and F. C. Walsh: J. Power Sources 160 (2006) 716. https://doi.org/10.1016/j.jpowsour.2006.02.095
- 8 D.-J. Park, K.-S. Jeon, C.-H. Ryu, and G.-J. Hwang: J. Ind. Eng. Chem. **45** (2017) 387. https://doi.org/10.1016/j.jiec.2016.10.007
- 9 X. Ke, J. M. Prahl, J. I. D. Alexander, J. S. Wainright, T. A. Zawodzinski, and R. F. Savinell: Chem. Soc. Rev. 47 (2018) 8721. https://doi.org/10.1039/C8CS00072G
- 10 B.-R. Kim, D.-Y. Sohn, Y.-H. Choi, and Y.-H. Lee: Appl. Sci. **10** (2020) 929. https://doi.org/10.3390/app10030929
- 11 J.-Y. Park, D.-Y. Sohn, and Y.-H. Choi: Appl. Sci. 10 (2020) 8427. https://doi.org/10.3390/app10238427
- 12 C.-H. Tian, R. Chein, K.-L. Hsueh, C.-H. Wu, and F.-H. Tsau: Rare Met. **30** (2011) 16. https://doi.org/10.1007/s12598-011-0229-1
- 13 C. R. Dennison, E. Agar, B. Akuzum, and E. C. Kumbur: J. Electrochem. Soc. **163** (2016) A5163. https://doi.org/10.1149/2.0231601jes
- 14 S. Kumar and S. Jayanti: J. Power Sources 307 (2016) 782. https://doi.org/10.1016/j.jpowsour.2016.01.048
- 15 Q. Xu, T. S. Zhao, and P. K. Leung: Appl. Energy 105 (2013) 47. https://doi.org/10.1016/j.apenergy.2012.12.041
- 16 R. Cervantes-Alcalá and M. Miranda-Hernández: J. Appl. Electrochem. 48 (2018) 1243. https://doi.org/10.1007/s10800-018-1246-7
- 17 Z. W. Sun, Z. N. Duan, J. Q. Bai, and Y. Wang: J. Energy Storage **29** (2020) 101370. https://doi.org/10.1016/j.est.2020.101370
- 18 D. J. You, J. Y. Wei, X. J. Li, and J. Y. Lou: CIESC J. **70** (2019) 4437. https://doi.org/10.11949/0438-1157.20190558
- 19 D. J. You, H. M. Zhang, and J. A. Chen, Electrochim. Acta. **54** (2009) 6827. https://doi.org/10.1016/j.electacta.2009.06.086

About the Authors



Cheng-Hsien Kuo received his Ph.D. degree in mechanical engineering from National Yang Ming Chiao Tung University, ROC. He is currently an associate professor in the Department of Mold and Die Engineering at National Kaohsiung University of Science and Technology. His research interests include CAD/CAM/CAE, redox flow batteries, bio-optical sensors, and the joining of dissimilar materials. (chuckkuo@nkust.edu.tw)



Shang-Ching Chuang received his B.S. and M.S. degrees from National Kaohsiung University of Science and Technology, Taiwan, where he majored in mold and die engineering. He is currently a Ph.D. candidate. His research interests include flow battery systems, bipolar plate welding and sealing technologies, materials engineering, and system integration and sensing for energy applications.



Hung-Yu Chen received his B.S. and M.S. degrees from National Kaohsiung University of Science and Technology, Taiwan, where he majored in mold and die engineering. His research interests include finite element analysis, computational fluid dynamics, materials engineering, and anion exchange membrane water electrolysis technology.